

MEMBRANE STRUCTURE AT SYNAPTIC JUNCTIONS IN AREA CA1 OF THE RAT HIPPOCAMPUS

K. M. HARRIS* and D. M. D. LANDIS†

Neurology Service, Massachusetts General Hospital, Boston, MA 02114, U.S.A.

Abstract—In tissue from area CA1 of the rat hippocampus prepared for electron microscopic study by thin-sectioning, asymmetric synaptic junctions were found on dendritic spines, spiny dendritic shafts, and non-spiny dendritic shafts. In freeze-fractured preparations, aggregates of large particles were found on the extracellular half of the postsynaptic membrane at each of these synaptic junctions. Particle aggregate areas were measured and particle packing densities were computed at dendritic spine synapses and dendritic shaft synapses in area CA1, and compared to similar measures of particle aggregates on dendritic spines of cerebellar Purkinje cells. All of these CA1 and cerebellar synapses are excitatory and are thought to use glutamate as a neurotransmitter. There was a tendency for the dispersion of particles within individual aggregates to be less uniform in larger aggregates in both area CA1 and cerebellar cortex. Distinct particle-free zones could be distinguished in the center of particle aggregates on large "mushroom-shaped" spines in area CA1. There was no statistically significant difference between the particle densities at CA1 dendritic spines (2848 ± 863 particles/ μm^2) and CA1 dendritic shafts (2707 ± 718 particles/ μm^2). However, the average density of particles at cerebellar dendritic spine synapses (3614 ± 1081 particles/ μm^2) was significantly greater than at dendritic spine or shaft synapses found in area CA1.

Symmetric synaptic junctions were observed on the CA1 pyramidal cell somas and dendritic shafts in thin-sectioned preparations. These synapses typically exert an inhibitory action mediated by gamma-aminobutyric acid. In freeze-fracture preparations, large varicosities were found apposed to the pyramidal somal and dendritic membranes, but there were no specializations of particle distribution on either the extracellular or the cytoplasmic half of the fractured postsynaptic membranes. This finding parallels observations from freeze-fracture preparations of other GABAergic synapses in the central nervous system.

Freeze-fracture techniques have proved to be useful tools in the study of synaptic structure and function. At the frog neuromuscular junction, for example, clusters of particles arrayed on the cytoplasmic half of the fractured postjunctional membrane occur in roughly the same density and distribution as acetylcholine receptor sites.^{17,25} In rapidly frozen tissue, where the true outer surface of the membrane has been exposed by etching, these particles appear to extend to the membrane surface.^{18,19} At mammalian neuromuscular junctions, these characteristic particles appear to be approximately co-extensive with sites labeled by alpha-bungarotoxin.³⁴ Their density and their disposition within the membrane thus suggest that these particles correspond to the acetylcholine receptor proteins.

At a variety of less well-characterized synaptic junctions in the central nervous system, aggregates of

particles occur in the fractured postsynaptic membrane.^{13,22-24,26,31,38,39} By analogy to the neuromuscular junction, it has been supposed that these postsynaptic particles are also related to synaptic function. In support of this hypothesis, it has been found that the appearance of the postsynaptic membranes is similar at synapses which employ the same neurotransmitter. In the mammalian CNS, particle aggregates occur on the extracellular half of the postsynaptic membrane of excitatory synapses which are likely to be glutaminergic. Inhibitory synapses using gamma-aminobutyric acid (GABA) as a neurotransmitter consistently lack any particle specializations in either half of their postsynaptic membranes. These sites both contrast with the cholinergic neuromuscular junction, where the particle aggregate occurs on the cytoplasmic half of the postsynaptic membrane.

In area CA1 of the hippocampus, different neurotransmitters are also active at different synaptic locations. Excitatory activation of CA1 pyramidal cells and interneurons occurs in the apical and basilar dendritic fields and is likely to be mediated by glutamate.^{2-4,7,9,27,43,44} Inhibitory activation of pyramidal cells or interneurons occurs closer to the cell bodies or on dendritic shafts and is GABAergic.^{1,5,6,20,37,41} At many of these synapses, the

*Address correspondence to: K. M. Harris, Department of Neuroscience, Children's Hospital Medical Center, 300 Longwood Ave., Boston, MA 02115, U.S.A.

†Present address: Departments of Neurology, Developmental Genetics and Anatomy, Case Western Reserve University, School of Medicine, Cleveland, OH 44106, U.S.A.

Abbreviations: GABA, gamma-aminobutyric acid.

position of the junctional specializations and/or the shape of the related neuronal processes allows for unequivocal identification at the electron microscopic level.^{8,10,12,14,16,28,45} In this report we have examined the junctional specialization of these hippocampal synapses with thin-section and freeze-fracture techniques in order to further correlate structure, physiological activity, and transmitter type in the central nervous system. A quantitative comparison of particle densities at excitatory synapses in area CA1 with excitatory synapses in cerebellar cortex provided an opportunity to determine whether differences in particle distributions at CNS synaptic junctions occur and whether such differences can be related to neurotransmitter type, synaptic location or synaptic size. Preliminary results have been presented elsewhere.¹⁵

EXPERIMENTAL PROCEDURES

Adult rats of the Long-Evans strain were anesthetized with intraperitoneal sodium pentobarbital and perfused with fixatives containing 1 or 2% paraformaldehyde and 1.25 or 2.5% glutaraldehyde with 2 mM CaCl₂ in 0.1 M sodium cacodylate buffer at pH 7.35 and 37°C for 15–30 min. Two animals were perfused with 1% paraformaldehyde, 1% glutaraldehyde and 0.5% acrolein in the same buffer followed by 6% glutaraldehyde. All animals were left undisturbed for 1 h. Then the hippocampus was removed and sliced transversely to its longitudinal axis, and the cerebellum was sliced sagittally into 200 or 400 μ m slices.

Thin sections

Several specimens were postfixed in 1% osmium tetroxide in 0.1 M sodium cacodylate buffer at 22°C for 1 h. Some tissue was soaked in 1% tannic acid in 0.1 M sodium cacodylate buffer at 22°C for 1 h. These samples, and others not pre-soaked in tannic acid, were stained *en bloc* with uranyl acetate prior to dehydration and embedding in Epon 812.

Freeze-fracture

The 200 μ m slices were equilibrated through 12.5–25% glycerol in 0.1 M sodium cacodylate buffer and frozen between gold hats by immersion in melting Freon 22 (monochlorodifluoromethane) at –155 to –160°C. Complementary replicas were obtained in a Balzers 400 freeze-fracture apparatus, cleaned in Clorox, rinsed in water, picked up on formvar coated slot grids or copper mesh grids, and viewed in a JEOL 100 CX electron microscope.

Quantitation of particle densities

Micrographs of particle aggregates on CA1 dendritic spines and CA1 dendritic shafts from the hippocampus of 7 animals, and cerebellar Purkinje cell dendritic spines from the cerebellum of 4 of the same animals were enlarged approximately 150,000 times. These micrographs were scrambled, and coded so that counts, judgements of fixation quality, angle of tilt, and particle size measurements were made without specific knowledge of fixation conditions, or animal number.

The areas of each aggregate were measured and the particles were counted twice using a GRAF/PEN sonic digitizing tablet interfaced to a MINC PDP11 laboratory computer. Areas of discrete particle-free zones, like those shown in Fig. 5, were subtracted from the total aggregate area when computing the densities. The mean density of these 2 counts was computed. If more than 5% error in these two measures and counts occurred, a third measure and

count was obtained and all three were averaged. If more than 5% error still remained, the micrograph was removed from the sample as being too difficult to measure and count accurately. Six micrographs, including one cerebellar spine and five CA1 spines, were removed in this fashion because of particle overlap due to sharp shadowing angles or because the boundaries of the aggregate were not well-defined.

Fixation quality of each dendrite was judged excellent, good or fair on a low magnification negative of the same field from which the high magnification prints were made for quantitation. The evaluation of fixation quality was based on particle dispersion at non-junctional areas of the membrane. Regions of "excellent" membrane fixation had a uniform dispersion of particles on the cytoplasmic and extracellular halves of non-junctional membranes. "Good" fixation was characterized by some regions of non-uniform particle dispersion on the non-junctional membranes. "Fair to poor" fixation resulted in ridges of particles separated by large patches of particle-free areas on non-junctional membranes.

Each aggregate was also evaluated for angle of tilt with respect to the apparent plane of the photograph. Particle shadow lengths and the dark shadow due to tilt with respect to the electron beam were used to judge the angle at which the aggregates were viewed. The tilt angle was estimated as high (40°), medium (25°), low (10°), or none (0°).³³ Then the areas measured were increased through division and the densities were decreased through multiplication by the cosines of these angles.

Particle size was measured in eleven aggregates from each synaptic location that had favorable shadow angles. Twenty particles in each aggregate were measured perpendicular to the shadow angle with an eyepiece micrometer (total = 660 particles).

Statistical methods

The RS1 statistical package (Bolt, Beranek and Neuman, Cambridge, MA) was used to test differences in particle packing densities at different synaptic locations, between animals, or for different tilt angles, with an analysis of variance followed by pairwise comparisons using the *t* statistic. Before applying the *t* statistic, distributions were tested for normality with the Wilkes-Shapiro or Kolmogorov-Smirnov tests, and homogeneity of variance with an *F* test. A non-parametric χ^2 test was used to test whether fixation quality varied across animals. Spearman's rho (r_s) tested whether there were correlations between particle packing densities and fixation quality or the aggregate area available for quantitation.

OBSERVATIONS

The pyramidal cell layer of area CA1 was readily identified in freeze-fracture replicas, and was used as a reference for determining relative position of synaptic junctions in the dendritic fields. The proximal apical dendritic shafts could often be traced for 50–100 μ m from individual pyramidal cell bodies and synaptic features were studied along these connected segments. In the apical field approximately 100–300 μ m from the cell body level, shorter dendritic segments were classified as spiny or non-spiny, and presumed to belong to the spiny pyramidal cells or non-spiny interneurons, respectively. Similarly, the cell body later served as a reference in thin-sectioned preparations for comparisons. Dendritic spines on Purkinje dendrites in the molecular layer of the cerebellar cortex were studied for quantitative com-

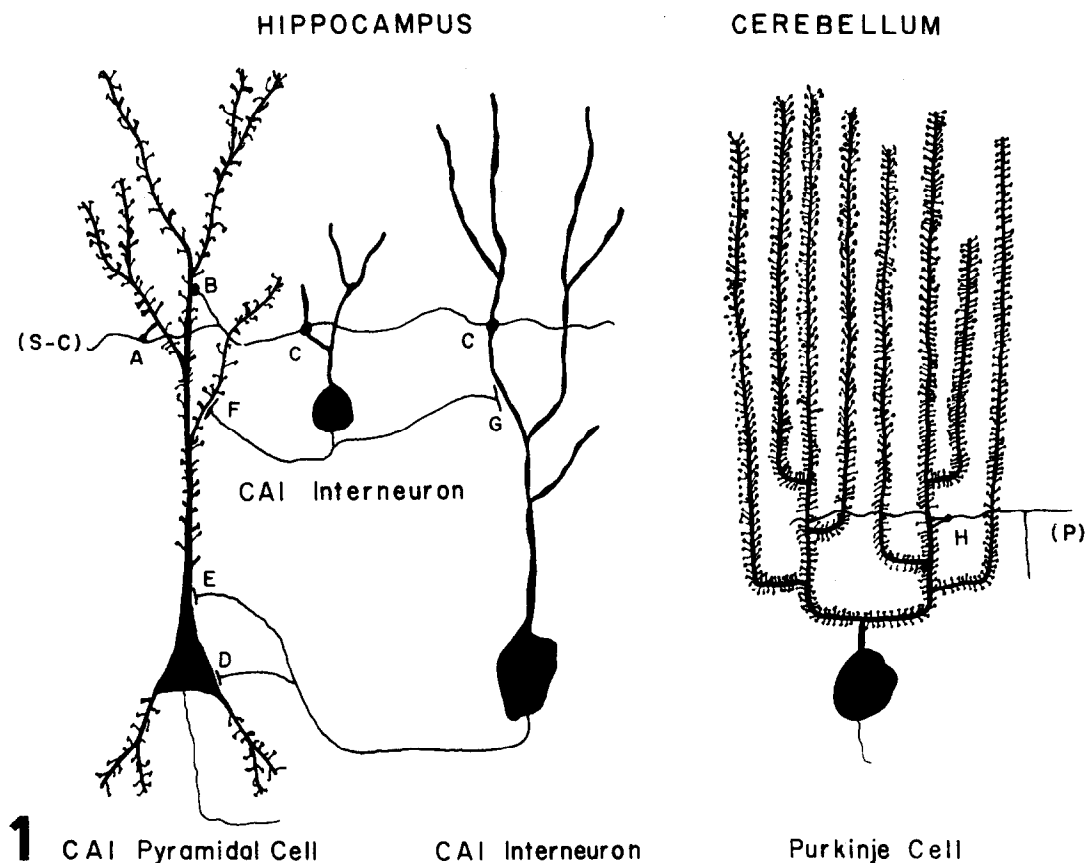


Fig. 1. Synapses studied in thin-sectioned and freeze-fractured preparations. The dendritic spines of CA1 pyramidal cells (A), dendritic shafts of spiny (B) and non-spiny neurons (C) form excitatory synapses with the Schaffer and commissural axons (S-C) from ipsi- and contralateral CA3 pyramidal cells (not shown here). Interneurons in area CA1 form inhibitory synapses with CA1 pyramidal cell bodies (D), proximal dendritic shafts (E), some distal spiny (F) and non-spiny dendritic shafts (G). Dendritic spines of cerebellar Purkinje cells form excitatory synapses (H) with parallel fibers (P) arising from granule cells (not shown here).

parisons of particle packing densities. These were identified on the basis of previously described criteria.²³ These synaptic locations are diagrammed in Fig. 1 in their relative positions, with presumed sources of afferent innervation.

Synaptic junctions on dendritic spines

There was a wide range in the variation of size and shape of dendritic spines in area CA1 of the hippocampus. In fortuitous fractures, nearby spines revealed in continuity with the parent dendrite ranged in size from small with a long, thin neck to relatively large and mushroom-shaped (Fig. 2). In thin-sectioned preparations, the small spines usually had a simple asymmetric synaptic junction, characterized by a dense postsynaptic thickening, a cleft with dense staining material and a presynaptic varicosity with round vesicles (Fig. 3). When viewed through serial sections, these postsynaptic thickenings appeared macular. Larger dendritic spines in area CA1 frequently had electron-lucent regions perforating the

electron-dense postsynaptic thickening (Figs 3 and 13), which had an overall annular or perforated shape when viewed through serial sections.

In freeze-fractured preparations, particles ranging in size from 6 to 17 nm could be found in aggregates on the extracellular half of the fractured spine membranes. In some fractures, these aggregates were seen adjacent to a widened synaptic cleft and a presynaptic varicosity filled with vesicles (Fig. 4). We studied 77 particle aggregates on CA1 dendritic spines and surveyed many other spine fragments where the aggregates were not visible. There was no evidence for presynaptic varicosities to be apposing the spine membranes in the absence of a postsynaptic particle aggregate. Often, particle aggregates were near the edge of a fractured membrane, so that some of the aggregate was not available for viewing. None the less, many such incompletely visualized aggregates could be characterized by the dispersion of particles within the aggregates as shown in Table 1. Aggregates with distinct particle-free zones were at the

Table 1. Particle dispersion within aggregates

Dispersion category	Number of particle aggregates in each dispersion category				Total
	1	2	3-6	0	
CA1 spines	31	27	9	10	77
Cerebellar spines	31	17	0	4	52
CA1 shafts	39	12	4	2	57

Dispersion categories: 1, uniform dispersion of particles in a macular aggregate; 2, non-uniform dispersion of particles in a macular aggregate; 3, uniform dispersion of particles around particle-free zones; 4, non-uniform dispersion of particles around particle-free zones; 5, uniform dispersion of particles in an anastomosing aggregate; 6, non-uniform dispersion of particles in an anastomosing aggregate; 0, aggregate broken and too small to classify by dispersion category.

extreme of a continuum of non-uniform particle dispersion within the aggregates. An example of this type of aggregate is illustrated in Fig. 5 and is likely to be a freeze-fracture equivalent of the perforated synapses seen in thin-section preparations.

When compared to the CA1 dendritic spines, Purkinje cell dendritic spines appeared more uniform in shape and size (Fig. 6), and particles ranging from 7 to 20 nm were dispersed more uniformly in macular aggregates (Fig. 7, Table 1).

Non-spiny dendritic shafts

In thin-sectioned preparations, many asymmetric synaptic junctions were found along non-spiny dendritic shafts in area CA1 and were characterized by a thick electron-dense postsynaptic specialization, a cleft with dense staining material, and a presynaptic varicosity with an accumulation of round vesicles (Fig. 8). There were also symmetric synaptic junctions on non-spiny dendrites, characterized by thin pre- and postsynaptic thickenings, dense staining cleft material and an accumulation of round and flattened vesicles in the presynaptic varicosity (Figs 8 and 11).

The extracellular half of the fractured membranes of non-spiny dendrites bore distinct aggregates of particles ranging in size from 7 to 23 nm (Fig. 9). All six categories of particle dispersion were observed, with the majority of particle aggregates having uniform particle dispersion in a macular pattern (Table 1). Non-spiny dendritic segments were typically apposed to several presynaptic varicosities, clustered adjacent to one another (Fig. 9). Some of these presynaptic varicosities had large particles on the cytoplasmic half of the fractured junctional membrane, and the contour of the varicosity appeared to be indented at the site of the junction. Other varicosities were relatively flat, with uniform particle dispersion on the cytoplasmic half of their membranes. These differences in presynaptic membrane structure might reflect differences in the rate of transmitter release during the interval of fixation, and/or different types of axons. In some instances, the particle aggregate on the extracellular half of the

fractured dendritic membrane was seen to be co-extensive with a widened junctional cleft and apposed to a cross-fractured presynaptic varicosity containing vesicles (Fig. 10). Less frequently, a presynaptic varicosity was observed in apposition to the extracellular half of fractured non-spiny dendritic membrane without evidence of a postsynaptic particle aggregate; these probably correspond to the symmetric synaptic junctions (Fig. 10, cf. Fig. 11).

Asymmetric junctions on spiny dendritic shafts

Occasionally, we observed particle aggregates on the extracellular half of fractured spiny dendritic shaft membranes (Fig. 12). These were assumed to represent synaptic junctions, although in no case was the presynaptic component visible. In thin-sectioned preparations, asymmetric junctions were also observed less often on spiny dendritic shafts than on the non-spiny dendritic shafts (Fig. 13).

Quantitation of particle packing densities

We calculated the particle packing densities in aggregates on CA1 dendritic spines and CA1 dendritic shafts and compared these with the packing density found on cerebellar dendritic spines. Figures 14 and 15 illustrate dendritic spines from area CA1 and cerebellar cortex at the actual magnification that was used to count particles. Outlines of the measures and counts that were obtained using a lighted magnifying ring over each picture are also illustrated. Both of these aggregates were classified in dispersion category 2, with estimated tilt angles of 25° and 0°, respectively.

In area CA1, the order of particle packing densities across dispersion categories for aggregates on dendritic spines was category 1 > 3-6 > 2 > 0 (see Table 1 for dispersion category definitions). Only category 0 was significantly less than the other categories ($t = 3.14$, $P < 0.005$), and the combined mean (\pm SD) for categories 1-6 was 2848 ± 863 particles/ μm^2 . Particle packing densities in aggregates on spiny dendritic shafts did not differ significantly from that in aggregates on non-spiny dendritic shafts. The order of particle packing densities at these CA1 shaft aggregates was dispersion category 1 > 2 > 3-6 > 0. None of these differences were significant, and the combined mean for categories 1-6 was 2707 ± 718 particles/ μm^2 . For cerebellar dendritic spines, particle packing density in category 1 was insignificantly greater than category 2 and the combined mean was 3614 ± 1081 particles/ μm^2 .

The mean particle packing density in aggregates on cerebellar dendritic spines was significantly greater than at CA1 spines ($t = 4.21$, $df = 113$, $P < 0.001$) and at CA1 dendritic shafts ($t = 4.93$, $df = 80$, $P < 0.0001$). These differences were also significant when dispersion categories 1 and 2 were compared separately across the three regions. Particle packing densities in aggregates at CA1 dendritic spines and dendritic shafts did not differ significantly. For all

Fig. 2. Dendritic spines on CA1 pyramidal cells. The plane of fracture has exposed the cytoplasmic half of the membrane of a CA1 dendritic shaft and two dendritic spines arising from it. The first spine (open square) is large and mushroom-shaped with the base at the dendritic shaft. The second spine (closed square) is smaller and lollipop-shaped with the stem at the dendritic shaft. In the head of the second spine, there are pits in the cytoplasmic half of the membrane adjacent to a widened synaptic cleft which are about the same diameter as the particles in the extracellular half of the membrane (closed circle). A third spine (closed triangle) on a neighboring dendritic is similar to the second spine in size and shape. Magnification as in Fig. 3.

Fig. 3. Two neighboring dendritic spines in a thin-sectioned preparation of the same region. The synaptic junction of the smaller spine (closed square) has a dense postsynaptic thickening adjacent to a synaptic cleft containing osmophilic material and a presynaptic varicosity with round vesicles. The postsynaptic thickening of the synaptic junction on the larger spine is perforated by electron lucent regions (open square). Bar = 0.5 μ m for Figs 2-7.

Fig. 4. Particle aggregate on an area CA1 dendritic spine. The particles aggregated on the extracellular half of the spine head membrane (closed square) are co-extensive with the widened synaptic cleft and a cross-fractured presynaptic varicosity. Magnification as in Fig. 3.

Fig. 5. Particle aggregate on CA1 dendritic spine. There are particle-free zones within the aggregate (open squares), which may correspond to the electron-lucent zones seen in junctions such as that in Fig. 3 (open square). Magnification as in Fig. 3.

Fig. 6. Purkinje cell dendritic spines. The fracture has exposed the cytoplasmic half of the membrane of two cerebellar dendritic spines (closed squares), one of which is apposed to a cross-fractured parallel fiber varicosity (closed circle). Magnification as in Fig. 3.

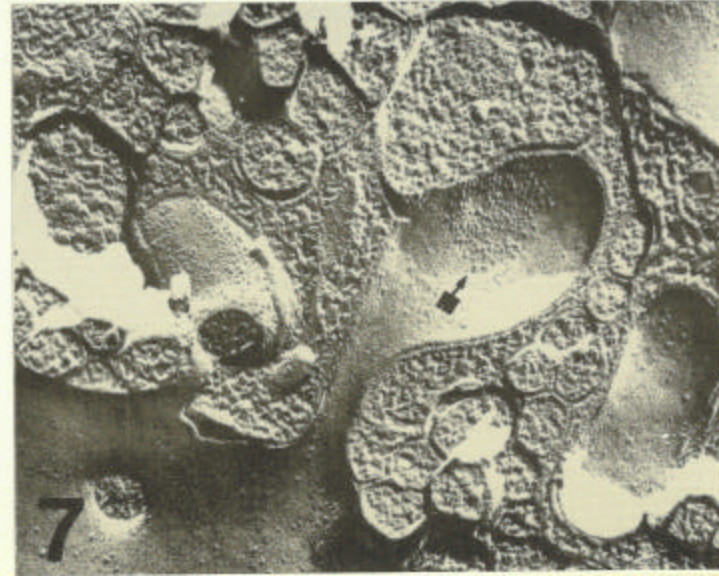
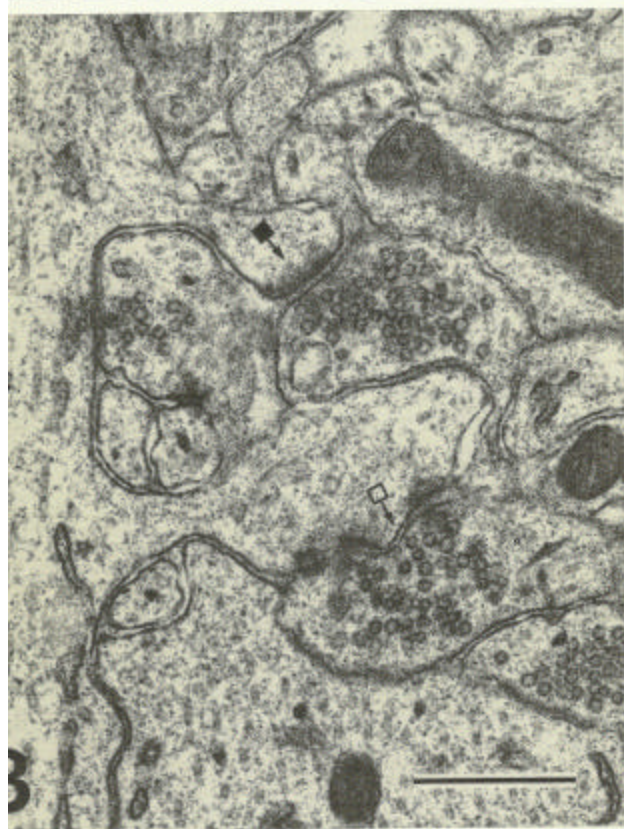
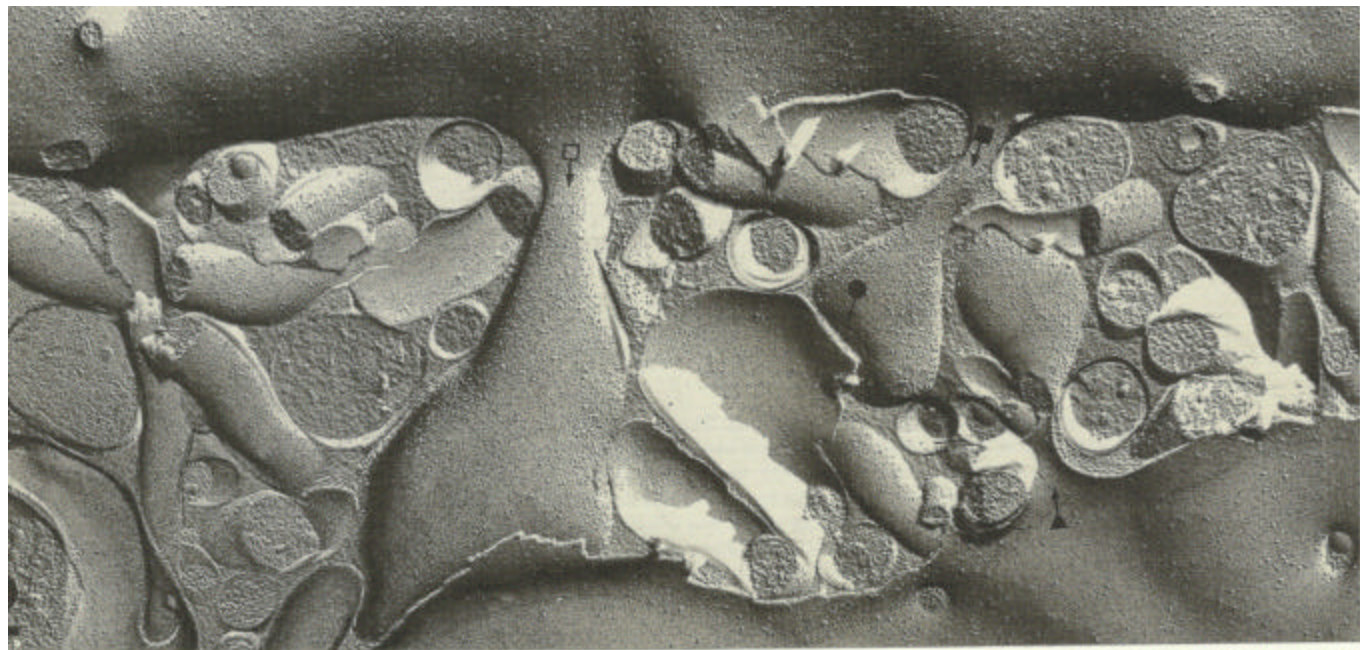
Fig. 7. Particle aggregate on a Purkinje cell dendritic spine. The aggregate on the extracellular half of the spine membrane is macular (closed square), without particle-free zones, and is adjacent to a vesicle-filled varicosity. Magnification as in Fig. 3.

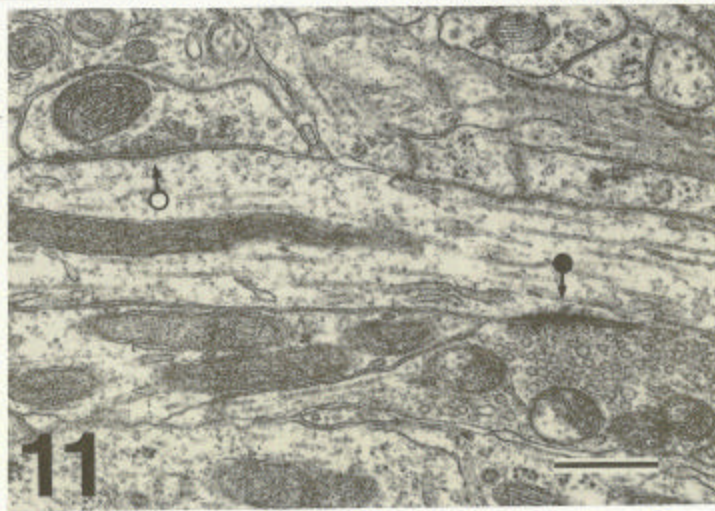
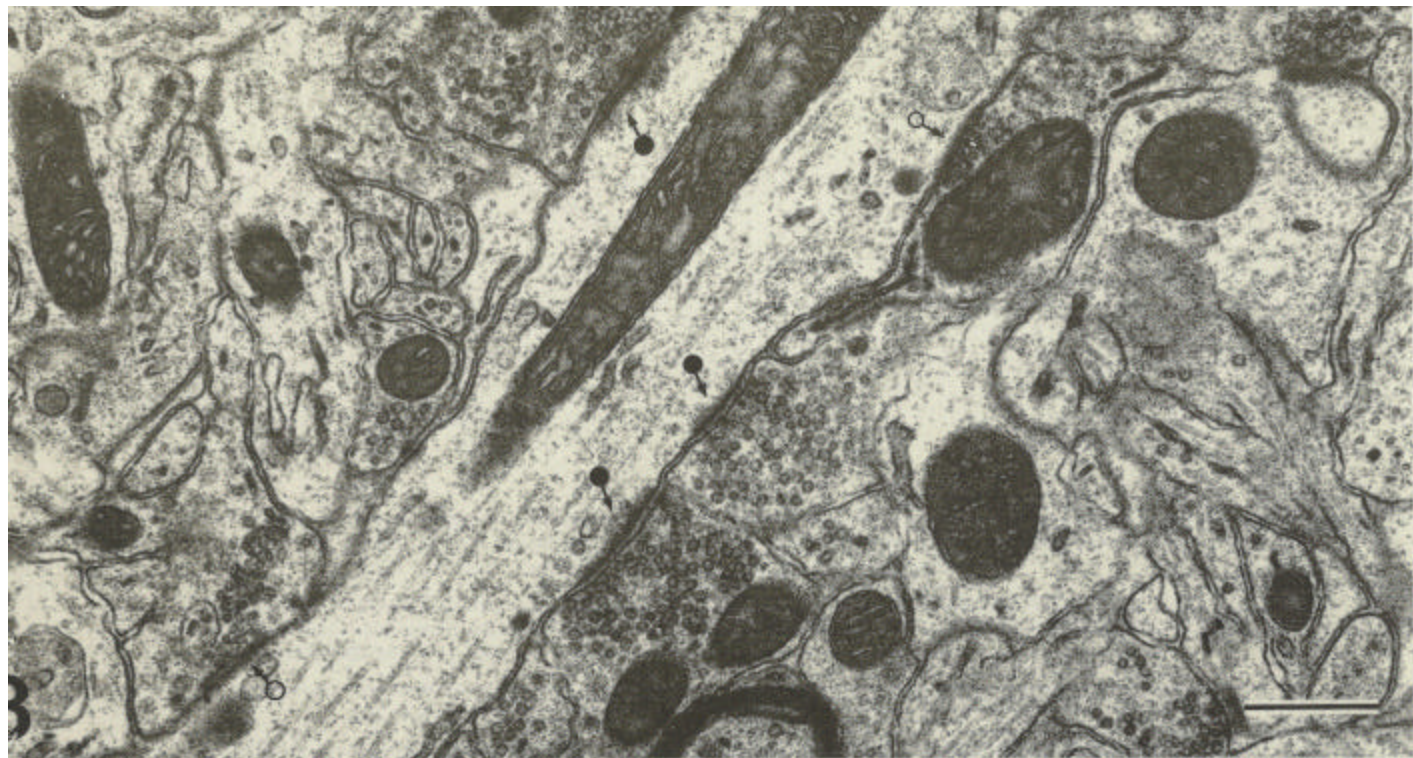
Fig. 8. Non-spiny dendritic shaft in area CA1. The dendritic shaft has three asymmetric synaptic junctions (closed circles) with presynaptic varicosities containing round vesicles. Two other junctions have been sectioned obliquely, and the vesicles of the presynaptic varicosities are oval and round (open circles). Bar = 0.5 μ m for Figs 8 and 9.

Fig. 9. Presynaptic varicosities adjacent to a segment of non-spiny dendritic shaft in area CA1. Two particle aggregates are visible on the extracellular half of the fractured dendritic shaft membrane (closed circles). The varicosities indicated by the stars are aligned along the course of the dendrite and probably formed synapses with it. Magnification as in Fig. 8.

Fig. 10. Non-spiny dendritic shaft in area CA1 with a particle aggregate. The aggregate (closed circle) appears to be co-extensive with a cross-fractured varicosity filled with vesicles. On the same dendritic segment, a portion of the fractured membrane adjacent to another varicosity does not have evidence of a particle aggregate (open circle), but in this instance, the precise location of the junction may not be included. Magnification as in Fig. 11.

Fig. 11. Synaptic junctions (closed circle) on a non-spiny dendrite in area CA1. The separation between the symmetric synaptic junction (open circle) and asymmetric synaptic junction (closed circle) is approximately the same as the separation of the two varicosities shown in Fig. 10. Bar = 0.5 μ m for Figs 10 and 11.





0

11

Fig. 12. Particle aggregate on a spiny shaft in area CA1. A large particle aggregate with a particle-free zone (closed circle) on the extracellular half of the dendritic membrane is located near the base of a dendritic spine origin (closed square). Magnification as in Fig. 13.

Fig. 13. Asymmetric synaptic junctions on a spiny CA1 dendrite. Two asymmetric synaptic junctions are present on the shaft of the dendrite (closed circles). The origin of a large, mushroom-shaped spine is indicated by closed squares. The large spine has a "perforated" synaptic junction. Bar = 0.5 μ m.

Fig. 14. Particle aggregate on a CA1 dendritic spine. The inset shows the number and distribution of counted particles on the fractured spine membrane. Magnification as in Fig. 15.

Fig. 15. Particle aggregate on a Purkinje cell dendritic spine. The inset shows the number and distribution of counted particles used in statistical analyses. Bar = 0.5 μ m.

Fig. 16. Symmetric synaptic junctions on CA1 pyramidal cell bodies. Two symmetric synaptic junctions on adjacent pyramidal cell bodies are characterized by thin pre- and postsynaptic thickenings separated by a cleft with electron-dense material (open circles). There is an accumulation of round and ellipsoidal vesicles in the presynaptic varicosity. Bar = 0.5 μ m.

Fig. 17. Symmetric synaptic junction on the proximal dendritic shaft of a CA 1 pyramidal cell. The details of the junctional specialization are like those illustrated in Fig. 16 (open circle). Magnification as in Fig. 16.

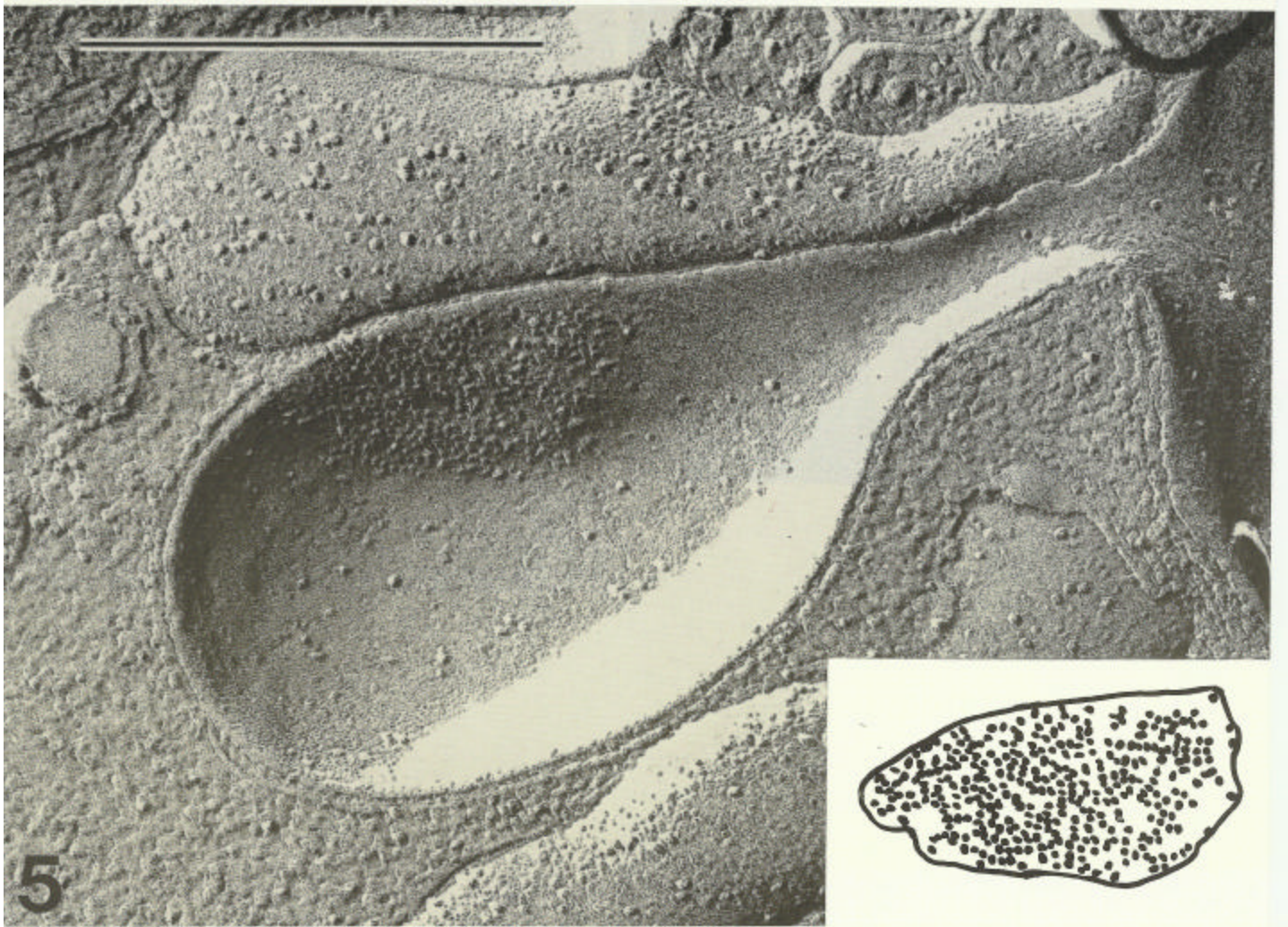
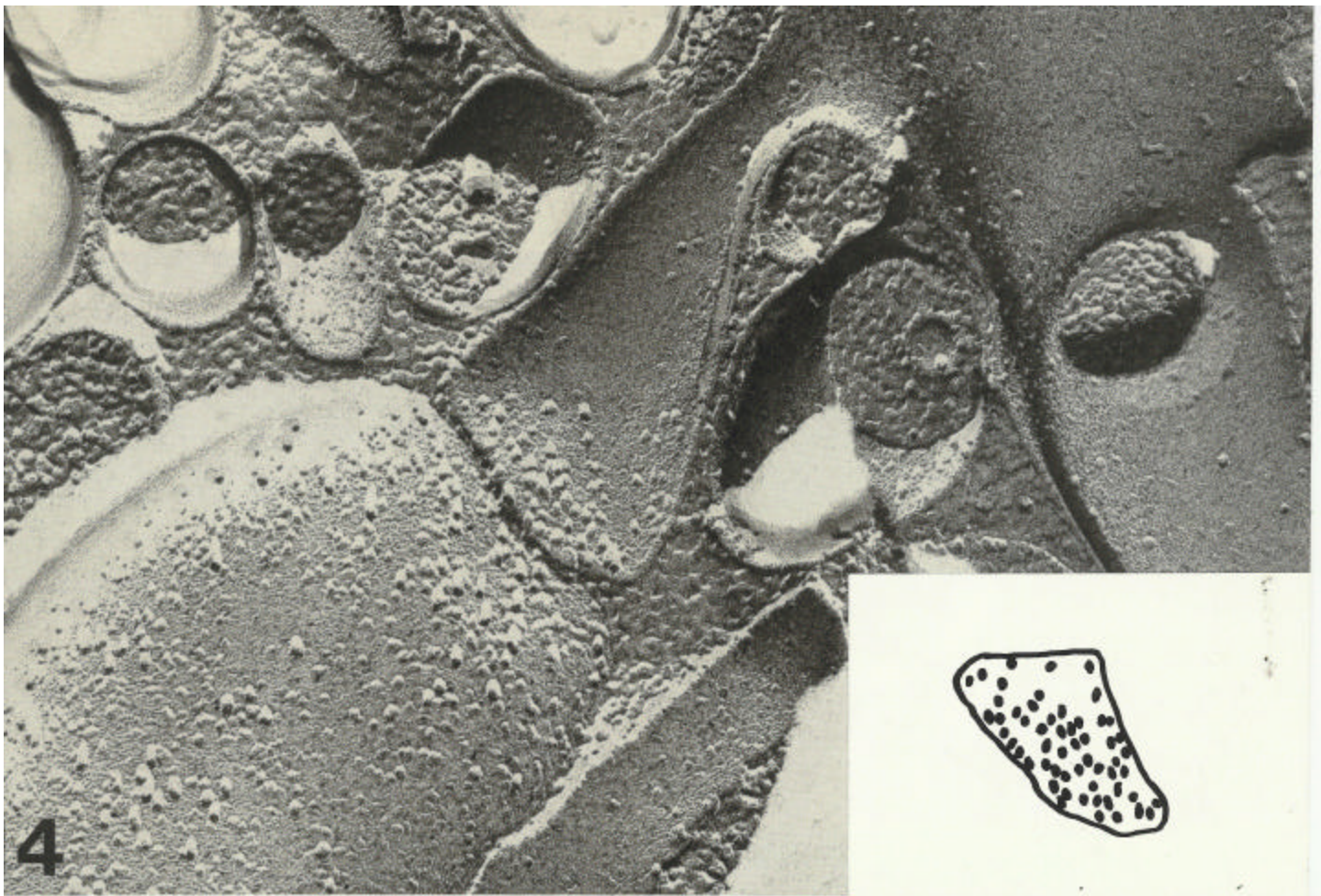
Fig. 18. Extracellular half of the fractured CA1 pyramidal cell membrane adjacent to a vesicle-filled varicosity. The open circles indicate two vesicle-filled varicosities, each juxtaposed to the soma of a pyramidal cell. There is no specialization of particle distribution on the extracellular half of the membrane, even in the immediate vicinity of the axonal varicosity. The site of the synaptic junction of the lower varicosity is revealed by the vesicles fused with the presynaptic membrane (large arrows). Magnification as in Fig. 16.

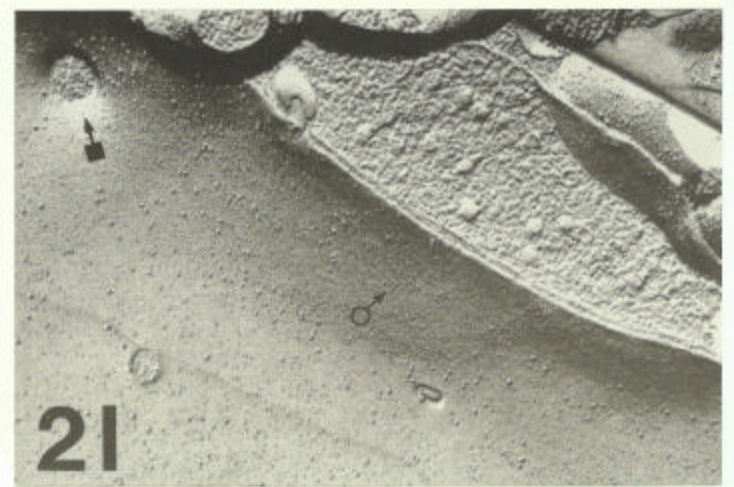
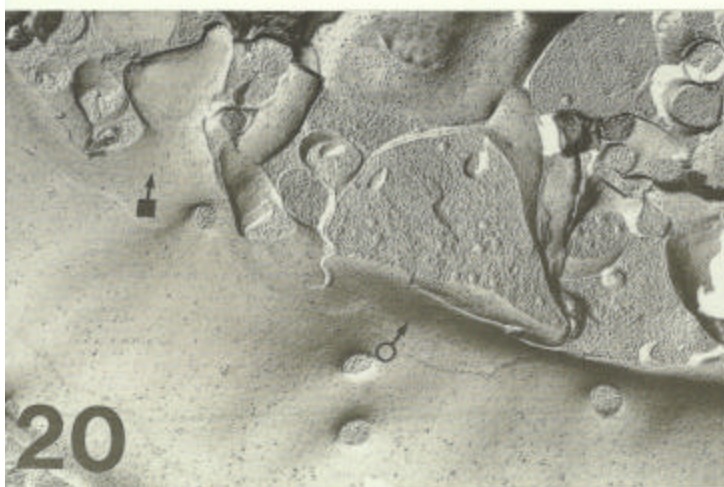
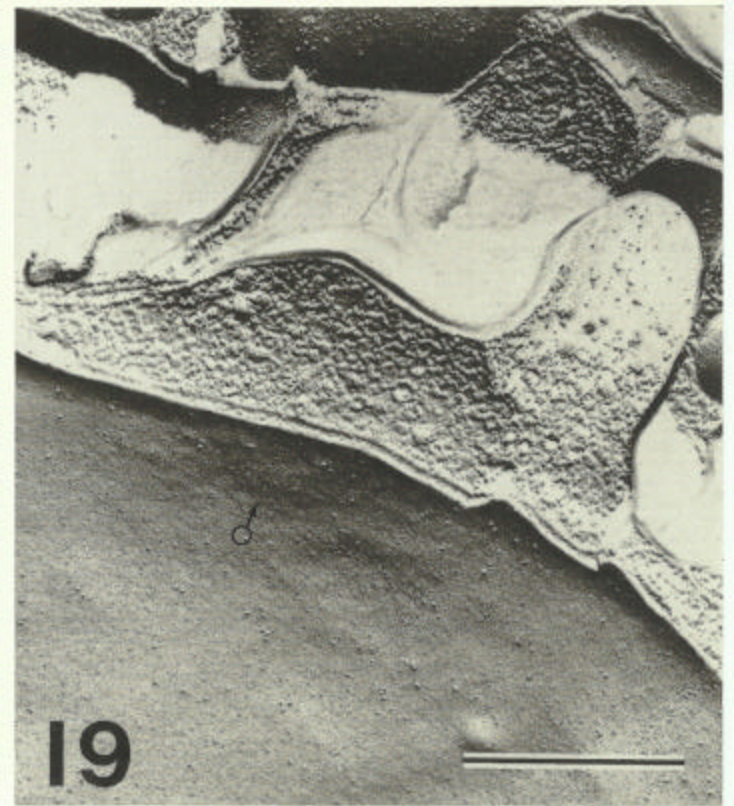
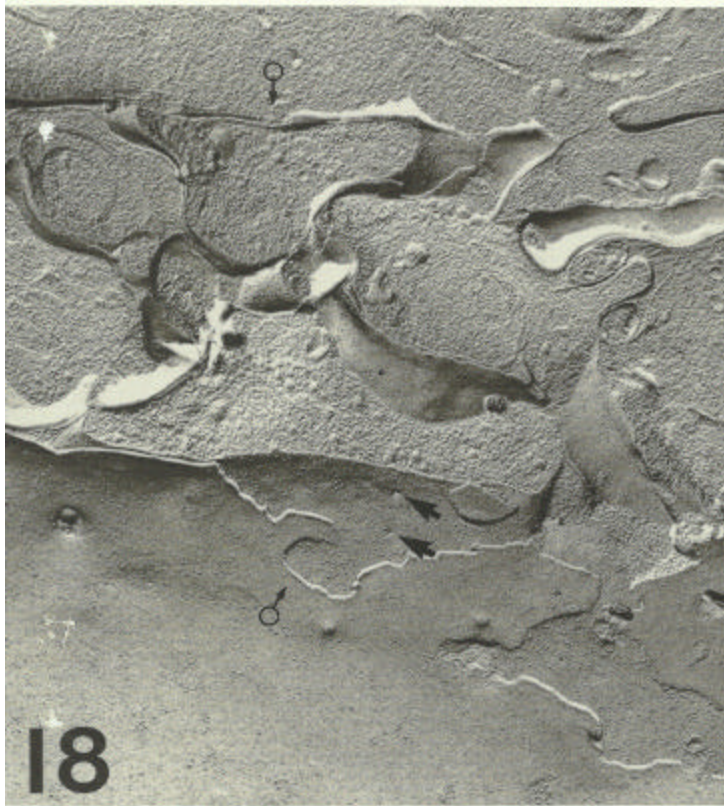
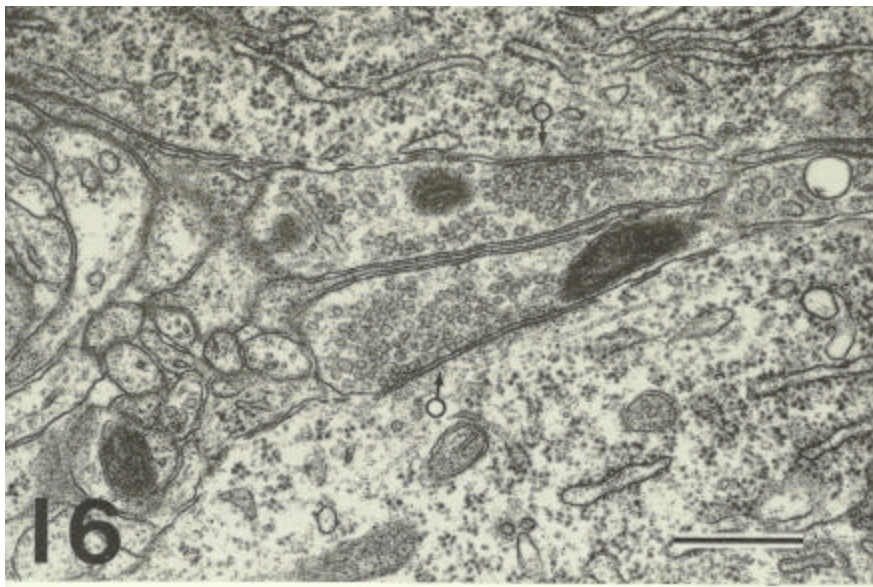
Fig. 19. Vesicle-filled varicosity adjacent to a CA1 pyramidal cell body. Intramembrane particles are widely dispersed over the extracellular half of the fractured membrane, and no aggregation or specialization of the particles is evident in the region coextensive with the varicosity. Bar = 0.5 μ m.

Fig. 20. CA1 Spiny dendritic shaft with apposed axonal varicosity. There is no specialization of particle distribution on the extracellular half of the membrane in the vicinity of the vesicle-filled varicosity (open circle). The origin of a spine is indicated by the closed square. Magnification as in Fig. 16.

Fig. 21. Spiny dendritic shaft with apposed axonal varicosity. No specialization of particle distribution is found in the extracellular half of the fractured membrane adjacent to a vesicle-filled varicosity (open circle). A closed square indicates the location of a dendritic spine origin. Magnification as in Fig. 19.







regions combined, particle packing density decreased with increasing aggregate area ($r = -0.24$, $df = 182$, $P < 0.001$).

Particle packing densities at these synaptic junctions were not influenced by fixation quality (see Experimental Procedures, quantitation of particle densities). In the brain of a single animal, different parts of single hippocampal or cerebellar replicas revealed areas of excellent, good, or fair fixation. Qualitative observations suggested, however, that fixation did not change the location of particle aggregates. Even in poorly fixed regions, discrete particle aggregates could be found on dendritic spines and on the shafts of non-spiny or spiny neurons at synaptic locations. Some of these were photographed and included in the quantitative analysis of particle densities. For CA1 spines, dendritic fixation varied significantly across animals ($\chi^2 = 62.31$, $df = 12$, $P < 0.001$), but fixation quality did not correlate with particle packing densities in the synaptic aggregates ($r_s = 0.08$, $P > 0.1$). For CA1 dendritic shafts and for cerebellar dendritic spines, the fixation quality did not vary significantly across animals and also did not correlate with particle packing densities in the synaptic aggregates.

The mean particle packing density at each of the four tilt angles was not significantly different for any of the 3 regions. There were no significant differences in particle packing densities between the 4 animals used to study both area CA1 and cerebellum. Three additional animals were used to complete the study of area CA1, and they produced a statistically insignificant increase in the mean particle packing densities at CA1 spine and shaft synapses.

Synapses on CA1 pyramidal cell bodies and apical dendritic shafts

In thin-sectioned preparations, symmetric synaptic junctions on the pyramidal cell bodies and on the spiny dendritic shafts were characterized by thin electron-dense submembrane material on both presynaptic and postsynaptic processes, and a slightly widened cleft containing electron-dense material. The presynaptic varicosity contained both round and flattened vesicles (Figs 16 and 17). In freeze-fracture preparations, vesicle-filled varicosities were frequently found in apposition to the pyramidal cell bodies and spiny dendritic shafts (Figs 18 and 19). At these sites, the extracellular half of the pyramidal cell membrane was indistinguishable from surrounding non-junctional membrane, where particle distribution was uniform and relatively sparse. The cytoplasmic half of the pyramidal cell membrane was similar to that illustrated in Fig. 2 of the spiny CA1 dendritic shaft, where particles are densely and uniformly distributed over both junctional and non-junctional regions.

In some instances, the cytoplasmic half of the presynaptic varicosity had large pits at the sites where vesicles had fused with the presynaptic membrane

(Fig. 18). These vesicle fusion sites provided a precise guide to the location of the active zone of the axonal varicosity. Varicosities were also found apposed to the spiny apical dendritic shafts. At these sites the extracellular half of the membrane had uniform and sparsely distributed particles like those seen at the cell bodies (Figs 20 and 21).

DISCUSSION

Synapses thought to exert an excitatory action at CA1 dendritic spines and dendritic shafts have asymmetric, electron-dense junctional specializations when viewed in thin-sectioned preparations and an aggregate of particles on the extracellular half of the postsynaptic membranes in freeze-fracture preparations. The particle packing density and overall shape of particle aggregate at CA1 synapses are more diverse than at cerebellar spine synapses, and range from uniform packing in essentially macular aggregates to non-uniform packing in anastomosing aggregates. There was also a tendency for particle dispersion within individual aggregates on CA1 spines, CA1 shafts or cerebellar spines to be less uniform in larger aggregates. Particle packing density was greater in aggregates on cerebellar dendritic spines than in aggregates on either CA1 dendritic shafts. Synapses thought to exert an inhibitory action at the CA1 pyramidal cell somas or dendritic shafts have symmetric electron-dense junctional specializations in thin-sectioned preparations. There were no specializations of particle distribution on either half of the postsynaptic membrane at these junctions in freeze-fracture preparations.

Despite overall similarities in the appearance of particle aggregates at excitatory synapses, quantitative analyses showed that there are important differences between hippocampal and cerebellar excitatory synapses. Particle packing densities in aggregates at hippocampal dendritic spine and shaft synapses are significantly less than those of synapses on Purkinje cell spines, even though all these synapses are thought to utilize glutamate as a neurotransmitter.^{27,40,42,44} The differences are not due to vagaries of fixation or to anomalies caused by shadowing angles, and are not simply a function of overall aggregate shape. These results suggest that the nature of the neurotransmitter is not solely responsible for the patterns of particle distribution occurring in the postsynaptic membrane. There are many possible explanations for the differences in particle packing densities, including differences in glutamate receptor subtypes in hippocampus and cerebellum, or the influence of other proteins found in the postsynaptic membrane.^{7a,9a}

A wide range in particle packing density has been described in the postsynaptic membranes of several synapses. If one limits consideration to junctional specializations with a macular shape, it has been reported that the particle packing density

of the glutaminergic excitatory synapse of primary auditory afferents on principal cells in the anteroventrocochlear nucleus is 1888 ± 156 particles/ μm^2 .¹³ This density is less than both area CA1 synapses and cerebellar spine synapses. Invertebrate neuromuscular junctions known to be excitatory and to use glutamate as a neurotransmitter have been studied in freeze-fracture preparations. In the moth, *Manduca sexta*, particles about 9 nm in size form aggregates in the extracellular half of the post-synaptic membrane with a density of 4080 ± 730 particles/ μm^2 .³⁶ In contrast, the glutaminergic neuromuscular junction of the locust, *Schistocerca gregaria*, has a particle packing density of only 480 particles/ μm^2 on the extracellular half of the postsynaptic membrane.²⁹ These values are almost completely outside the range of values we found for CNS glutaminergic synapses and may reflect differences between the CNS and neuromuscular synapses or phylogenetic differences, even though the neurotransmitter seems to be the same.

The reasons for the heterogeneity of particle packing density in macular aggregates are unknown. It is possible that the differences between hippocampal and cerebellar synapses are a reflection of differences in the proportions of glutamate receptor sub-types, though there is no direct evidence to show that any of the aggregated particles are receptors. Nevertheless, if particles represent receptors and/or ion channels, then particle packing densities and the shape of the aggregate might be related to synaptic function. At the frog neuromuscular junction, it seems likely that the particles arrayed on the cytoplasmic half of the fractured postsynaptic membrane actually represent acetylcholine receptor sites, partly because the particle density corresponds fairly well to the estimated receptor density.²⁵ Particle densities in freeze-fracture preparations of other systems have been related to possible functions of the intramembranous proteins they are thought to represent. For example, Pumplin *et al.*³³ have measured an average density of 1500 ± 300 particles/ μm^2 on the cytoplasmic half of the presynaptic membrane of the squid giant synapse. Calculations assuming that one particle represented a single Ca^{2+} channel have a computed channel conductance of 0.2 pS for each channel ("particle"). This value compared favorably with measured estimates of 0.06–0.6 pS for Ca^{2+} channels obtained from physiological studies of the same synapses. The extracellular half of the post-synaptic membrane of the squid giant synapse had a density of 2000 ± 400 particles/ μm^2 in an aggregate.

For these particles, they calculated a conductance of 2.1 pS/particle, a value in the range of that expected for $\text{Na}^+ - \text{K}^+$ channel in these same synapses.

Particles are not always uniformly dispersed within the aggregates at synaptic junctions. Non-uniform dispersion might result from uneven partitioning of proteins when the membrane is fractured.³⁵ In areas without obvious particles, the protein might have been cleaved, or pulled out of the membrane to the complementary side and therefore not be visible as a particle.³² An alternative, more likely, explanation is that the particle-free regions are the freeze-fracture representation of the electron-lucent regions seen in the postsynaptic density of some synapses in thin-sectioned preparations.^{9b} This explanation is supported by the more frequent observations of non-uniform particle dispersion on large CA1 dendritic spines. In thin-sectioned preparations these large spines frequently have postsynaptic densities with electron-lucent perforations.⁴⁵ In the frog cerebellum, large particle aggregates on granule cell dendritic shafts have particle-free zones in them and smaller shaft aggregates have more uniform particle dispersion.²¹ Thus, there is a general tendency for particle dispersion to be non-uniform in larger aggregates. The reasons for this tendency are not apparent. It has been suggested that "perforated" synaptic junctions on hippocampal dendritic spines represent a stage in the division of the junction,³⁰ but our observations add little further evidence to that suggestion.

In area CA1, like other CNS structures, inhibitory synapses have synaptic junctions with no obvious specializations of particle distribution on either the cytoplasmic or extracellular half of the fractured membrane. Presumably, intramembranous particles associated with synaptic function at these junctions either cleave such that they are unrecognizable, or partition with the cytoplasmic half of the membrane and are there in sufficiently low numbers that they cannot be discerned against the high background of non-junctional particles.

Acknowledgements—We thank Larry Cherkas and Bill McIntosh for photographic assistance, and Lori Weinstein for technical assistance. Dr Max Snodderly participated in many useful discussions of the results, and together with Dr Robert Goldstein provided advice and assistance with statistical analyses, using the RS1 statistical program at The Eye Research Institute of the Retina Foundation, Boston, Massachusetts. This investigation was supported by NS 15573 (DMDL), NIH postdoctoral fellowship NS 07082 (KMH), and NS 21184 (KMH).

REFERENCES

1. Alger B. E. and Nicol R. A. (1982) Feed forward dendritic inhibition in rat hippocampal pyramidal cells studied *in vitro*. *J. Physiol.* **328**, 105–123.
2. Anderson P. (1960) Interhippocampal impulses II. Apical dendritic activation of CA1 neurons. *Acta physiol. scand.* **48**, 178–208.
3. Anderson P., Blackstad T. W. and Lomo T. (1966) Location and identification of excitatory synapses on hippocampal pyramidal cells. *Expl Brain Res.* **1**, 236–248.

4. Anderson P., Bliss T. and Skrede K. (1971) Lamellar organization of hippocampal excitatory pathways. *Expl Brain Res.* **13**, 222–238.
5. Anderson P., Eccles J. and Loyning Y. (1964) Location of postsynaptic inhibitory synapses on hippocampal pyramids. *J. Neurophysiol.* **27**, 592–607.
6. Anderson P., Eccles J. C. and Loyning Y. (1964) Pathway of postsynaptic inhibition in the hippocampus. *J. Neurophysiol.* **27**, 608–619.
7. Anderson P., Silfvenius H., Sundberg S. H. and Sveen O. (1980) A comparison of distal and proximal dendritic synapses on CA1 pyramids in guinea pig hippocampal slices *in vitro*. *J. Physiol.* **307**, 273–299.
- 7a. Banker G., Churchill L. and Cotman C. W. (1974) Proteins of the postsynaptic density. *J. Cell Biol.* **63**, 456–465.
8. Blackstad T. W. (1963) Ultrastructural studies on the hippocampal region. *Prog. Brain Res.* **3**, 122–148.
9. Buzsaki G. and Eidelberg E. (1982) Direct afferent excitation and long-term potentiation of hippocampal interneurons. *J. Neurophysiol.* **48**, 597–607.
- 9a. Cohen R. S., Blomberg F., Berzins F. and Siekevitz P. (1977) The structure of the postsynaptic densities isolated from dog cerebral cortex. I. Overall morphology and protein composition. *J. Cell Biol.* **74**, 181–203.
- 9b. Cohen R. S. and Siekevitz P. (1978) Form of the postsynaptic density. A serial section study. *J. Cell Biol.* **78**, 36–46.
10. Frotscher M. and Zimmer J. (1983) Commissural fibers terminate on non-pyramidal neurons in the guinea pig hippocampus—a combined Golgi/EM degeneration study. *Brain Res.* **265**, 289–293.
11. Gayoso M. J., Diaz-Flores L., Garrido M., Sanchez G. and Velasco E. (1979) Hippocampal formation. IV. Interneurons. *Morfologia Normal y Patologica* **3**, 247–277.
12. Gottlieb D. L. and Cowan W. M. (1972) On the distribution of axonal terminals containing spheroidal and flattened synaptic vesicles in the hippocampus and dentate gyrus of the rat and cat. *Z. Zellforsch.* **129**, 413–429.
13. Gulley R. L., Landis D. M. D. and Reese T. S. (1978) Internal organization of membranes at end bulbs of Held in the anteroventral cochlear nucleus. *J. comp. Neurol.* **180**, 707–742.
14. Hamlyn L. H. (1963) An electron microscope study of pyramidal neurons in the Ammons horn of the rabbit. *J. Anat., Lond.* **97**, 189–201.
15. Harris K. M. and Landis D. M. D. (1983) Freeze-fracture study of membrane structure in the CA1 region of rat hippocampus. *Soc. Neurosci. Abst.* **9**, 341.6.
16. Harris K. M., Marshall P. E. and Landis D. M. D. (1985) Ultrastructural study of cholecystokinin-immunoreactive cells and processes in area CA1 of the rat hippocampus. *J. comp. Neurol.* **233**, 147–158.
17. Heuser J. E., Reese T. S. and Landis D. M. D. (1974) Functional changes in frog neuromuscular junctions studied with freeze fracture. *J. Neurocytol.* **3**, 109–131.
18. Heuser J. E. and Salpeter S. R. (1979) Organization of acetylcholine receptors in quick-frozen deep-etched and rotary-replicated *Torpedo* postsynaptic membrane. *J. Cell Biol.* **82**, 150–173.
19. Hirokawa N. and Heuser J. E. (1982) Internal and external differentiation of the postsynaptic membrane at the neuromuscular junction. *J. Neurocytol.* **11**, 487–510.
20. Knowles W. D. and Schwartzkroin P. A. (1981) Local circuit synaptic interactions in hippocampal brain slices. *J. Neurosci.* **1**, 318–322.
21. Korte G. E. and Rosenbluth J. (1980) Freeze-fracture study of the postsynaptic membrane of the cerebellar mossy fiber synapse in the frog. *J. comp. Neurol.* **193**, 689–700.
22. Landis D. M. D. (1982) Structure and function at synapses. *Trends Neurosci.* **5**, 215–216.
23. Landis D. M. D. and Reese T. S. (1974) Differences in membrane structure between excitatory and inhibitory synapses in the cerebellar cortex. *J. comp. Neurol.* **155**, 93–126.
24. Landis D. M. D., Reese T. S. and Raviola E. (1974) Differences in membrane structure between excitatory and inhibitory components of the reciprocal synapse in the olfactory bulb. *J. comp. Neurol.* **155**, 67–92.
25. Matthews-Ballinger J. and Salpeter M. M. (1978) Distribution of Ach receptors at frog neuromuscular junctions with a discussion of some physiological implications. *J. Physiol.* **279**, 197–213.
26. Mattox D. E., Neises G. R. and Gulley R. L. (1983) Species differences in the synaptic membranes of the end bulb of Held revealed with the freeze-fracture technique. *Anat. Rec.* **205**, 57–63.
27. Nadler J. V., Vaca K., White W. F., Lynch G. S. and Cotman C. W. (1979) Aspartate and glutamate as possible transmitters of excitatory hippocampal afferents. *Nature* **260**, 538–540.
28. Nafstad P. M. J. (1967) An electron microscope study on the termination of the perforant path fibres in the hippocampus and the fascia dentata. *Z. Zellforsch.* **76**, 532–542.
29. Newman T. M. and Duce I. R. (1983) Membrane specializations of the neuromuscular junction of the locust, *Schistocerca gregaria*. *Cell Tiss. Res.* **234**, 691–706.
30. Nieto-Sampedro M., Hoff S. F. and Cotman C. W. (1982) Perforated postsynaptic densities: probable intermediates in synapse turnover. *Proc. natn. Acad. Sci. U.S.A.* **79**, 5718–5722.
31. Pfenninger K., Akert K., Moor H. and Sandri C. (1972) The fine structure of freeze-fractured presynaptic membranes. *J. Neurocytol.* **1**, 129–149.
32. Pinto da Silva P. and Branton D. (1970) Membrane splitting in freeze-etching covalently bound ferritin as a membrane marker. *J. Cell Biol.* **45**, 598–605.
33. Pumpkin D. W., Reese T. S. and Llinas R. (1981) Are the presynaptic membrane particles the calcium channels? *Proc. natn. Acad. Sci. U.S.A.* **78**, 7210–7213.
34. Rash J. E., Johnson T. J. A., Hudson C. S., Giddings F. D., Graham W. F. and Eldefrawi M. E. (1982) Labelled-replica techniques: Post-shadow labelling of intramembranous particles in freeze-fracture replicas. *J. Microscopy* **128**, 121–138.
35. Rash J. E. and Hudson C. S. (1979) *Freeze Fracture: Methods, Artifacts and Interpretations*. Raven Press, New York.
36. Rheuben M. B. and Reese T. S. (1978) Three-dimensional structure and membrane specializations of moth excitatory neuromuscular synapse. *J. Ultrastruct. Res.* **65**, 95–111.
37. Ribak C. E., Vaughn J. E. and Saito K. (1978) Immunocytochemical localization of glutamic acid decarboxylase in neuronal somata following colchicine inhibition of axonal transport. *Brain Res.* **140**, 315–332.
38. Sandri C., Akert K., Livingston R. B. and Moor H. (1972) Particle aggregations at specialized sites in freeze-etched postsynaptic membranes. *Brain Res.* **41**, 1–16.
39. Sandri C., Van Buren M. and Akert K. (1977) Membrane morphology of the vertebrate nervous system. *Prog. Brain Res.* **46**, 1–384.

40. Schulman J. A. (1983) Chemical neuroanatomy of the cerebellar cortex. In *Chemical Neuroanatomy* (ed. Emson P. C.), pp. 209–228. Raven press, New York.
41. Somogyi P., Smith A. D., Nunzi M. G., Gorio A., Takagi H. and Wu J. Y. (1983) Glutamate decarboxylase immunoreactivity in the hippocampus of the cat: distribution of immunoreactive synaptic terminals with special reference to the axon initial segment of pyramidal neurons. *J. Neurosci.* **3**, 1450–1468.
42. Stone T. W. (1979) Glutamate as the neurotransmitter of cerebellar granule cells in the rat: electrophysiological evidence. *Br. J. Pharmac.* **66**, 291–296.
43. Storm-Mathisen J. (1977) Localization of transmitter candidates in the brain: The hippocampal formation as a model. *Prog. Neurobiol.* **8**, 119–181.
44. Walaas I. (1983) The hippocampus. In *Chemical Neuroanatomy* (ed. Emson P. C.), pp. 337–358. Raven Press, New York.
45. Westrum L. E. and Blackstad T. W. (1962) An electron microscopic study of stratum radiatum of the rat hippocampus (Regio superior, CA1) with particular emphasis on synaptology. *J. comp. Neurol.* **119**, 281–309.

(Accepted 31 March 1986)